Evidence for correlated electron pairs and triplets in quantum Hall interferometers

Wenmin Yang, David Perconte, Corentin Déprez, Kenji Watanabe, Takashi Taniguchi, Sylvain Dumont, Edouard Wagner, Frédéric Gay, Inès Safi, Hermann Sellier, et al.

Evidence for correlated electron pairs and triplets in quantum Hall interferometers

Wenmin Yang,[1,*] David Perconte,[1,*] Corentin Déprez,[1] Kenji Watanabe,[2] Takashi Taniguchi,[3] Sylvain Dumont,[1] Edouard Wagner,[1] Frédéric Gay,[1] Inès Safi,[4] Hermann Sellier,[1] and Benjamin Sacépé[1,†]

[1] *Univ. Grenoble Alpes, CNRS, Grenoble INP, Institut Néel, 38000 Grenoble, France*
[2] *Research Center for Electronic and Optical Materials, National Institute for Materials Science, 1-1 Namiki, Tsukuba 305-0044, Japan*
[3] *Research Center for Materials Nanoarchitectonics, National Institute for Materials Science, 1-1 Namiki, Tsukuba 305-0044, Japan*
[4] *Université Paris-Saclay, CNRS, Laboratoire de Physique des Solides, 91405 Orsay, France*

Pairing of electrons is ubiquitous in electronic systems featuring attractive inter-electron interactions, as exemplified in superconductors [1]. Counter-intuitively, it can also be mediated in certain circumstances by the repulsive Coulomb interaction alone [2, 3]. Quantum Hall (QH) Fabry-Pérot interferometers (FPIs) tailored in two-dimensional electron gas under a perpendicular magnetic field has been argued to exhibit such unusual electron pairing seemingly without attractive interaction [4–7]. Here, we show evidence in graphene QH FPIs [8–11] revealing not only a similar electron pairing at bulk filling factor $\nu = 2$ but also an unforeseen emergence of electron tripling characterized by a fractional Aharonov-Bohm flux period $h/3e$ (h is the Planck constant and e the electron charge) at $\nu = 3$. Leveraging a novel plunger-gate spectroscopy, we demonstrate that electron pairing (tripling) involves correlated charge transport on two (three) entangled QH edge channels. This spectroscopy indicates a quantum interference flux-periodicity determined by the sum of the phases acquired by the distinct QH edge channels having slightly different interfering areas. While recent theory invokes the dynamical exchange of neutral magnetoplasmons –dubbed neutralons– as mediator for electron pairing [12], our discovery of three entangled QH edge channels with apparent electron tripling defies understanding and introduces a new three-body problem for interacting fermions.

The quantum Hall effect is known to host a wide range of correlated and symmetry protected phases. Coulomb repulsion plays a central role in it, shaping the structure of QH edge channels [13], inducing (pseudo) spin-polarized QH ferromagnets [14], or generating fractional quantum Hall states [15] with anyonic excitations that may be useful for topological quantum computation [16].

In 2015, a surprise came with the observation of pairing of electrons in QH interferometers. Choi and coworkers [4] found in GaAs Fabry-Pérot interferometers defined by two quantum point contacts in series [17] an anomalous Aharonov-Bohm effect with halved flux-periodicity, $h/2e$. The specific configurations identified were the presence of at least two QH edge channels in the FPI, that is, a bulk filling factor $\nu > 2$, and interference from the outer channel while the inner is localized in a closed loop. Strikingly, this electron pairing was confirmed by quantum shot noise that evidenced an effective charge $e^* \sim 2e$ (Refs. [4, 7]), pointing conspicuously towards correlated electron-pair transport.

The analogy with Cooper pairing as in superconductors is tantalizing, however the resemblance is only apparent since there is no attractive, non-coulombic interaction, nor evidence of a macroscopic condensate. On the theoretical front, most efforts to date have failed to describe this baffling phenomenon [12, 18, 19]. Yet, an effective dynamical pairing via the exchange of neutralons [12] has been put forward, but cannot capture all phenomenology [4, 5, 7].

Here, we opt for a different platform –the graphene QH FPI [8, 9] to uncover new insights into this phenomenon. By leveraging the high-tunablility of its plunger gate [8] and conducting systematic out-of-equilibrium transport measurements, we establish a new QH edge channel spectrometry that allows us to identify the exact channels involved coherently in the electron pairing. Furthermore, at filling factor $\nu = 3$, we uncover evidence of electron tripling involving coherent transport of three electrons over the three distinguishable edge channels. Our unprecedented systematic exploration of the flux and energy bias parameter space gives key insights into a complex interplay between edge channels and their interactions.

The graphene QH FPIs are made with hBN-encapsulated graphene deposited onto graphite gate acting as back-gate electrode. Two quantum point contacts (QPCs) are electrostatically defined by a set of two palladium split-gate electrodes [8, 21]. The FPIs are equipped with a plunger-gate electrode to tune the effective area enclosed by the QH edge channels. Several 1D ohmic contacts [22] allow us to source and drain current and probe voltages across the FPI. Figure 1a shows an atomic force microscopy topography of the device studied in the main text, which has a FPI cavity area of $2.2 \pm 0.2\,\mu\text{m}^2$. Importantly, the FPI is defined by the pristine, non-etched edges of the graphene flake, ensuring confinement of the

* These authors contributed equally to this work.
† benjamin.sacepe@neel.cnrs.fr

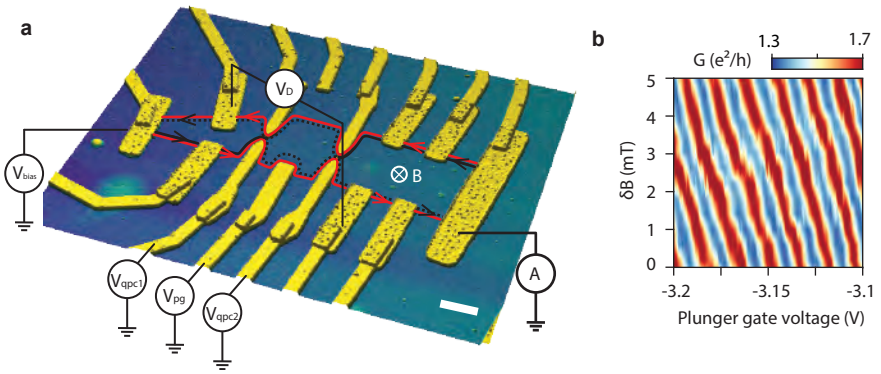

FIG. 1: Graphene quantum Hall Fabry-Pérot interferometer. **a**, Atomic force microscope image of the hBN encapsulated graphene heterostructure. Ohmic contacts are highlighted in yellow (with a rough surface), while quantum point contact (QPC) electrodes and the plunger gate are highlighted in light yellow (with a smooth surface). The inner and outer quantum Hall edge channels at a bulk filling factor of 2 are represented by black and red lines, respectively. In this configuration, the inner edge channel (dashed line) is partitioned by the QPCs. The measured diagonal voltage V_D and current give the diagonal conductance of the interferometer. **b**, Diagonal conductance oscillations as a function of magnetic field and plunger gate voltage, illustrating the interference of the inner edge channel (with a back-gate voltage of 1.8 V, i.e., $\nu_B = 2.26$), as schematically shown in (**a**). The negative slope of the constant phase lines indicates Aharonov-Bohm dominated interference [20].

QH edge channels to within a few magnetic lengths of the crystal edge, without any edge reconstruction [23], and by split and plunger gates. All experiments are performed at a magnetic field of 14 T and a temperature of 0.01 K. Partial pinch off of the inner channel as overlaid in Fig. 1a yields conductance oscillations shown in Fig. 1b with negative slope in the magnetic-field, B, versus plunger gate voltage, V_{pg}, plane, which is characteristic of Aharonov-Bohm quantum interference for a flux periodicity of h/e [8, 20].

Gate-spectroscopy fingerprint of QH edge channels

The considerable advantage of graphene FPI over conventional semiconductors is the absence of a bandgap, which allows very large electrostatic tuning of the charge carrier density from the electron states to the hole states. Figure 2d illustrates this tunability with conductance oscillations versus plunger-gate voltage, V_{pg}, from -5 to 0 V, reflecting the quantum interference of the inner channel at $\nu = 2$ (same configuration as in Fig. 1). The Fourier transform of these oscillations in a small sliding window gives the plunger-gate dependence of the oscillation frequency [8]. The resulting gate-spectroscopy shown in Fig. 2e reveals three peaks of decreasing amplitudes (see inset) that relate to the first harmonic frequency f_{pg} and the next two $2f_{pg}$ and $3f_{pg}$. This indicates quantum interference occurring over two and three turns of the inner channel loop, thus providing a clear signature for the interferometer's high coherence. Importantly, each peak diverges at the same plunger gate voltage $V_{pg}^c = -0.28$ V, which corresponds to the expulsion of the inner channel from under the gate when the filling factor under the gate reaches $\nu_{pg} \sim 1$. This divergence is channel-specific [8] and provides an unambiguous indicator of the QH edge channels involved in the interference.

One new aspect of our measurement lies in the systematic acquisition of IV curves at each point of interference pattern in Fig. 2d (or in Fig. 1b), enabling us to simultaneously explore the complete parameter space of energy, gate voltage, and magnetic field (see Supplementary Video 1 [24]). Figure 2d is actually extracted at zero bias from the bias-dependence data. The oscillation yields a checkerboard pattern as a function of bias voltage, illustrated in Fig. 2b in a restricted gate range, reflecting the additional phase shift acquired by the injected electrons at finite energy. In turn, this enables us to compute the Fourier transform of the oscillations at each bias voltage (see Supplementary Video 2 [24]) and extract the bias voltage dependence of each harmonics that we display in Fig. 2f. The resulting oscillatory lobe structure of each harmonics is best fitted with a Gaussian decay for the energy relaxation (see Ref. [8]), and provides the Thouless energy of the interferometer edge $E_{Th} = hv/L = 135$ μV (bias-oscillation period), where $L = 3.4$ μm is the length of the interfering channel between two QPCs and v the edge-excitation velocity. The harmonics then yield E_{Th}/N (see Fig. 2f inset), where N is the respective harmonic index, providing an assessment of $v = 1.1 \times 10^5$ m.s^{-1} consistent with our previous work [8].

Electron pairing on two coherently coupled channels

Electron pairing emerges in our interferometer in presence of two edge channels by interfering with the outer

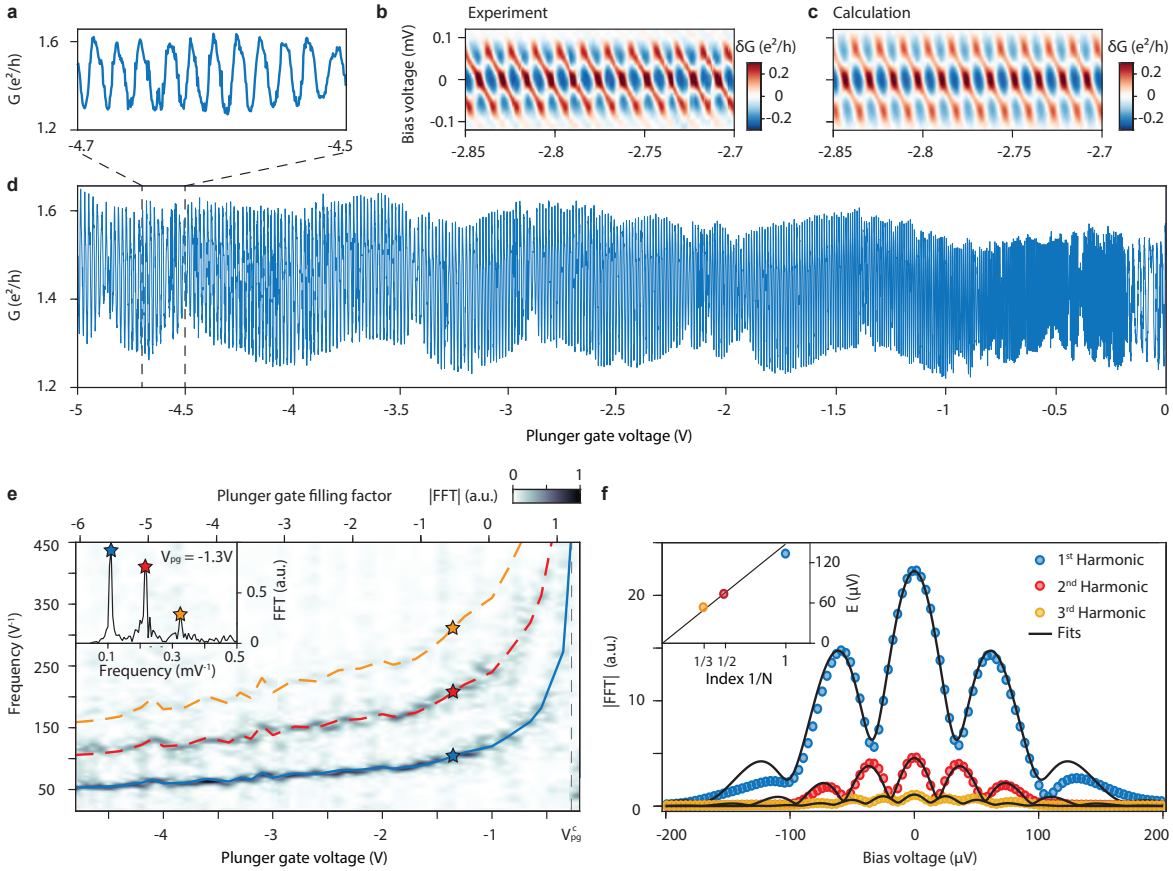

FIG. 2: Gate-spectrocopy of inner channel Aharonov-Bohm interference a, Diagonal conductance as a function of plunger-gate voltage $V_{\rm pg}$. **b**, Checkerboard pattern of the conductance oscillation as a function of $V_{\rm pg}$ and dc bias voltage. **c**, Calculated checkerboard pattern in the presence of three harmonics (see Methods). **d**, Full plunger-gate scan of the conductance oscillation as a function of $V_{\rm pg}$ measured at a back-gate voltage of 1.8 V ($\nu_{\rm B} = 2.26$). The dc voltage bias dependence of those oscillations are shown in Supplementary Video 1 [24]. **a** and **b** are extracted from the data in **d**. **e**, Fourier transform of **d** computed over a sliding window in $V_{\rm pg}$, as a function of plunger gate voltage. This gate spectroscopy is obtained here at dc bias voltage of -28 μV. Supplementary Video 2 [24] shows the entire energy dependence of the Fourier transform. The blue solid line highlights the first oscillation harmonic. Dashed lines colored in red and yellow are calculated as twice and three times the blue line, respectively, indicating the second and third oscillation harmonics. The inset is the Fourier transform at fixed $V_{\rm pg} = -1.3$ V, which shows three harmonic peaks labeled with with blue, red and yellow stars, respectively. **f**, Lobe structure of the three Fourier harmonics, showing the energy dependence of their amplitudes. Inset: Thouless energy, extracted from the fit of the lobe structure (see Methods), is nearly linear with the inverse of harmonic index.

channel while keeping the inner channel localized in the interferometer cavity (see Fig. 3a inset schematics). Gate-spectroscopy shown in Fig. 3a reveals the pairing frequency (green dashed line) that is almost twice that of the inner channel interference shown previously in Fig. 2e. Since an area variation of one flux quantum is $\Delta A = \phi_0/B = \alpha \Delta V_{\rm pg} = \alpha/f_{\rm pg}$, where α is the (nonlinear) lever arm of the gate and $\Delta V_{\rm pg}$ the plunger-gate oscillation period, a frequency doubling therefore signals an abnormal flux periodicity of $h/2e$ similar to that reported in GaAs [4, 5, 7].

The frequency doubling is also evidenced by the presence of a residual peak at half the frequency highlighted with a red dashed line that coincides with the frequency of the outer channel h/e-periodic interference, the latter being independently characterized by its spectroscopy at a different filling factor where pairing is sub-dominant. Inspecting the plunger gate-evolution of those frequencies, we see that both pairing and outer channel frequencies diverge at $V_{\rm pg}^{\rm c} = -0.96$ V that corresponds to a filling factor underneath the plunger gate $\nu_{\rm pg} = 0.05$, in agreement with the expulsion of the outer channel from the plunger gate area.

However, unlike the harmonics in Fig. 2e, the pairing frequency is not exactly twice that of the outer channel: At $V_{\rm pg} = -4.8$ V, one finds 105 V^{-1} and 45 V^{-1}, respec-

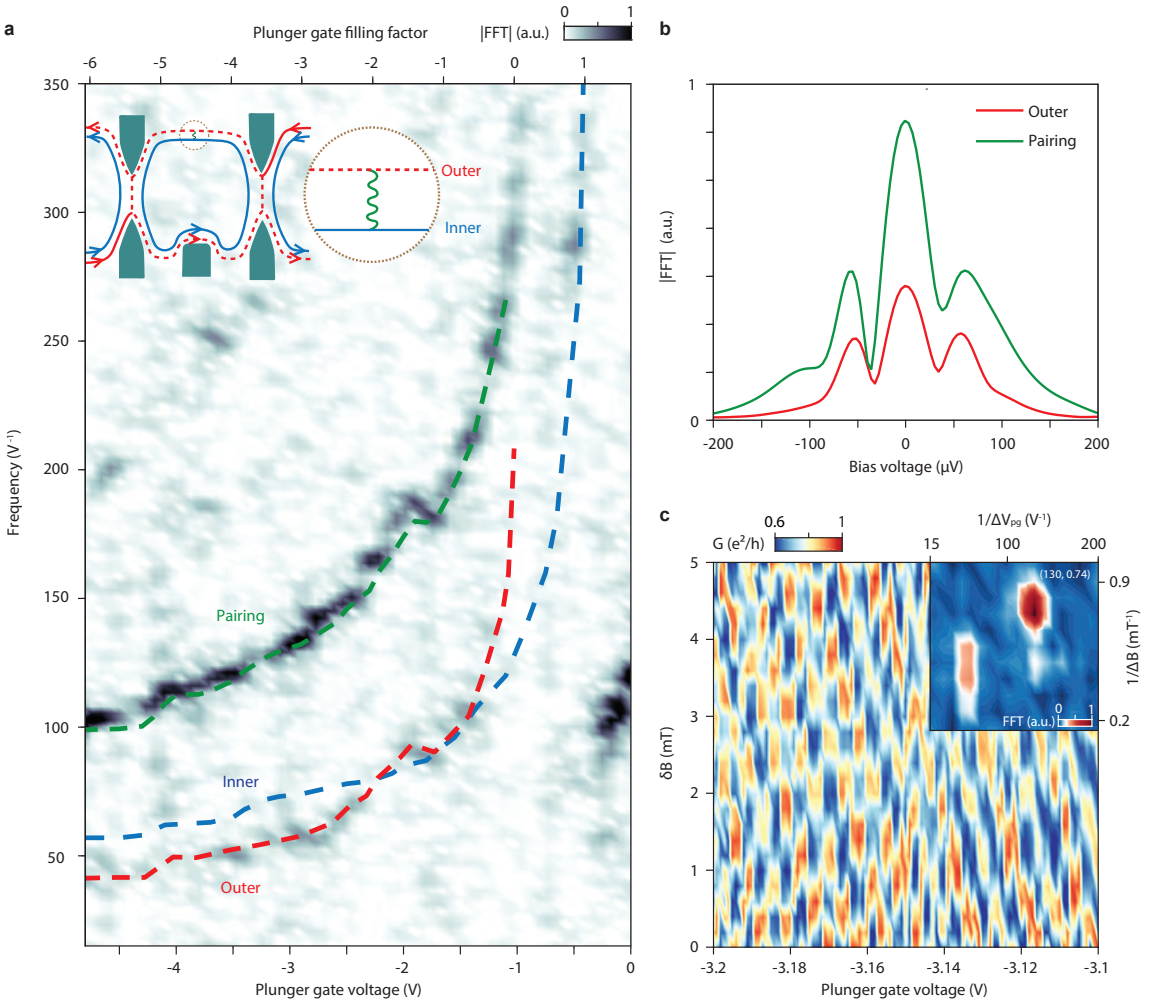

FIG. 3: Gate-spectroscopy of pairing interference. **a**, Fourier transform (FT) amplitude of the conductance oscillation of the outer edge channel versus plunger-gate voltage and plunger-gate oscillation frequency, at $V_{\rm bg} = 1.8$ V ($\nu_{\rm B} = 2.26$) and dc bias voltage of -55.5 μV. Supplementary Video 3 [24] shows the dc bias voltage dependence of it. The blue and red dashed lines represent the oscillation frequencies of the inner and outer interfering edges, respectively. The green dashed line is the sum of these two frequencies. The edge channel configuration is shown in the inset schematics, where the partitioned outer channel is labeled with a red dashed line, and the green wavy line represents the interaction between inner and outer edge channels. **b**, Lobe structure of the Fourier amplitude of the pairing (red colored) and outer (green colored) channel frequencies as a function of dc bias voltage, extracted from the data in **a**. **c**, Diagonal conductance oscillation –pajama map– showing the beating between outer and pairing frequencies at zero bias (Supplementary Video 4 [24] shows the full bias-voltage dependence of the same data). The inset is a 2 dimensional Fourier transform of the pajama map showing the outer and pairing frequencies.

tively. To understand this discrepancy we add on the gate-spectroscopy the inner channel frequency (first harmonic measured in Fig. 2e) as a blue dashed line, which leads us to a central finding of this study: The pairing frequency is not the double of the Aharonov-Bohm frequency but the sum of the distinct inner and outer channels frequencies. This is clearly seen with the green dashed line in Fig. 3a, which is actually constructed from the sum of the blue (inner channel) and red (outer channel) dashed lines, and which fits remarkably well the pairing frequency dispersion. Here the different frequencies for the inner and outer channels stem from their slightly different positions with respect to the plunger and QPC split gates, quantified in SI Fig. S3 (see Methods), and thus their different effective areas.

This finding is particularly striking and insightful as it demonstrates that, although localized, the inner channel contributes coherently to the quantum interference of the outer channel, and thus to this unusual pairing frequency. It further implies that the pairing involves excitations propagating on both inner and outer channels, thus picking up the sum of the Aharonov-Bohm phases of

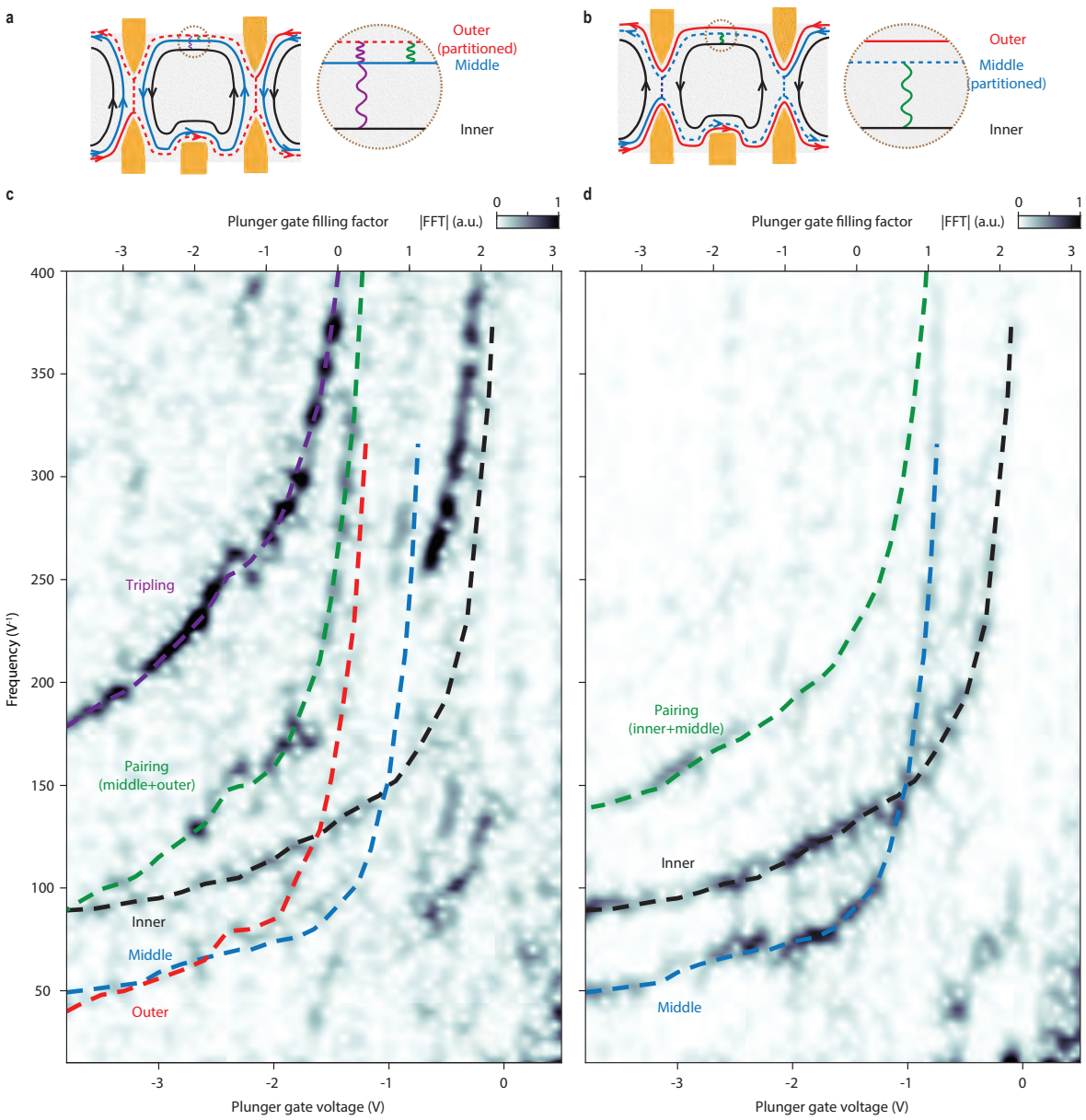

FIG. 4: Tripling and pairing interference. **a** and **b**, Schematic illustrations of the edge channel configurations for the tripling in **a** with outer channel intefering and pairing in **b** with middle channel interfering. The inner, middle and outer edges are color-coded in black, blue and red, respectively. Dashed lines indicate the partitioned edge. The green wavy line depicts the interaction between middle and outer edge channels, while the purple wavy line illustrates the interactions among all the three edges. **c** and **d**, Gate-spectroscopy computed from the conductance oscillations of the outer **c** and middle **d** interfering edge channels, as a function of plunger gate voltage and plunger gate oscillation frequency. In both cases the back-gate voltage is 2.5 V ($\nu_B = 2.93$). Top axis indicates the filling factor underneath the plunger gate. The black, blue and red dashed lines represent the oscillation frequencies of the inner, middle and outer edges, respectively. In **c**, the green dashed line (pairing signal) is the sum of middle and outer edge frequencies, and the purple dashed line (tripling signal) is the sum of all three channel frequencies. In **d**, the green dashed line is the frequency sum of the inner and middle edge channels. **a** and **b** are extracted at zero bias and -55 μV, respectively. The bias voltage dependence of the gate spectroscopy **c** and **d** are shown in Supplementary Videos 5 and 6 [24].

both channels $\varphi = \frac{h}{e}\oint_{inner} \mathbf{A}.\mathbf{dl} + \frac{h}{e}\oint_{outer} \mathbf{A}.\mathbf{dl}$, where $\mathbf{A}$ is the vector potential.

Examining the energy-dependence of this gate-spectroscopy displayed in Fig. 3b shows that the pairing and the outer channels exhibit nearly the same voltage-bias periodicity, that is, Thouless energy, confirming the

fact that the pairing frequency is not an harmonic of the outer channel interference. Here, the pairing clearly prevails over the h/e-periodic outer channel contribution but we show in Extended Data Fig. 1 that the relative contribution of the pairing increases and becomes dominant when the filling factor increases.

Notably, the zero-bias pajama map shown in Fig. 3c exhibits a distinctive discontinuous pattern, deviating from the standard Aharonov-Bohm pajama shown in Fig. 1b. This pattern results from the addition of the pairing and outer channel oscillations, each contributing with specific weights given in Fig. 3b. The Fourier transform in Fig. 3c inset reveals the two contributions with a doubling of both the gate and magnetic field frequencies. The energy-evolution of this frequency mixing is shown in Supplementary Video 4 [24], highlighting the rich complexity that can emerge in these QH interferometry patterns.

Electron tripling on three coherently coupled channels

The observation of pairing naturally raises the question as to whether the inclusion of an additional third channel could lead to a threefold increase in frequency, namely, electron tripling, although this has not been observed thus far in GaAs [4–7].

To address this intriguing question we set our QH FPI to bulk filling factor 3 and, akin to the case of pairing, we partitioned the outer channel, while having the middle and inner channels localized (see Fig. 4a). Figure 4c displays the resulting plunger gate spectroscopy that reveals a new frequency, highlighted with the purple dashed line, almost three times higher than that of the outer channel: At $V_{\rm pg} = -3.9$ V, one finds 179 $\rm V^{-1}$ and 45 $\rm V^{-1}$, respectively. By overlaying the spectral dispersion of the inner (black), middle (blue) and outer (red) channels, each separately identified, we can calculate the sum of the three. This sum is represented by the purple dashed line and conspicuously overlaps with the tripling frequency. As for the case of pairing, the tripling frequency therefore results from the sum of the three distinct Aharonov-Bohm phases of the three edge channels, each characterized by different effective areas.

The coherent mixing and contributions of the three channels result in a pajama pattern shown in Supplementary Video 7 [24] that is even more complex than that for the pairing. Still, a reduction in the magnetic field periodicity to 1/3 the Aharonov-Bohm period is readily visible as compared to Fig. 1b and, interestingly, phase jumps also develop as the result of this multiple frequencies mixing.

Importantly, a non-negligible pairing contribution shown in green dashed line in Fig. 4c remains present and comes from the sum of the outer and middle channel frequencies. This suggests that pairing occurs only between the partitioned channel and the nearest neighbor channel, the middle one in this case. To ascertain this observation, we carried out another gate-spectroscopy in a different configuration in which we partitioned the middle channel, fully transmitted the outer channel and localized the inner channel (see Fig. 4b). The resulting spectroscopy displayed in Fig. 4d clearly shows a pairing contribution coming from the sum of the middle and inner channels frequencies, confirming that this pairing occurs between partially and fully localized nearest neighbor channels.

Interestingly, the amplitude of the pairing peak is weaker in this configuration (confirmed also at slightly different filling factors in Fig. S5b), while the middle and inner frequencies are clearly visible. Here, the difference with the previous configuration at filling factor 2 is that the pairing involves channels belonging to two different Landau levels, that is, the zeroth and first Landau level. Consequently, the edge channels are more spatially separated due to the large cyclotron gap compared to the case of pairing between outer and middle, which both belong to the zeroth Landau level. The fact that pairing intensity increases with smaller separations between channels strongly suggests that inter-channel Coulomb interaction plays a crucial role in the pairing and tripling.

A key question to assess the Coulomb interaction quantitatively is the real space distance between edge channels. As in optical interferometry, our gate-spectroscopy provides a very accurate measurement of the interfering path, which can in turn leads to the edge channel-to-gate distance $\delta(V_{\rm pg})$ by integrating the $V_{\rm pg}$-dependence of an edge channel frequency (see Methods). We show in Fig. 5d the resulting distances for the three channels at $\nu = 3$. Strikingly, despite a relatively smooth electrostatic potential, the outer (red line) and middle (blue line) channels are very close, with a distance δ on the order of or even smaller than the magnetic length $l_B = \sqrt{h/2\pi eB}$, implying strongly interacting channels. For instance we obtain $\delta = 5.6$ nm at $V_{\rm pg} = -3$ V with a magnetic length $l_B = 6.7$ nm at $B = 14$ T. On the other hand, the inner channel (black line) that belongs to the first Landau level is located at ~ 35 nm (at $V_{\rm pg} = -3$ V) away from the middle channel. This distance can be accounted for by the large cyclotron gap between the zeroth and first Landau levels of graphene. On the contrary, along the graphene crystal edges of the FPI, the QH edge channels are known to be all confined on a scale of the order of l_B to the crystal edge [23, 25]. We can thus outline the spatial structure of edge channels as well as the many-body Landau level spectra at the crystal edges and at the pn junctions in our FPI with the schematics in Fig. 5. This provides unprecedented and accurate measurements of the inter-channel distances, which are crucial for a further theoretical assessment of Coulomb interactions between the channels. It is also fully consistent with our observation and interpretation of weaker pairing between middle and inner channel at $\nu = 3$ discussed above.

Discussion

Inter-channel interactions are expected to induce charge redistribution in edge magnetoplasmons [28–30]

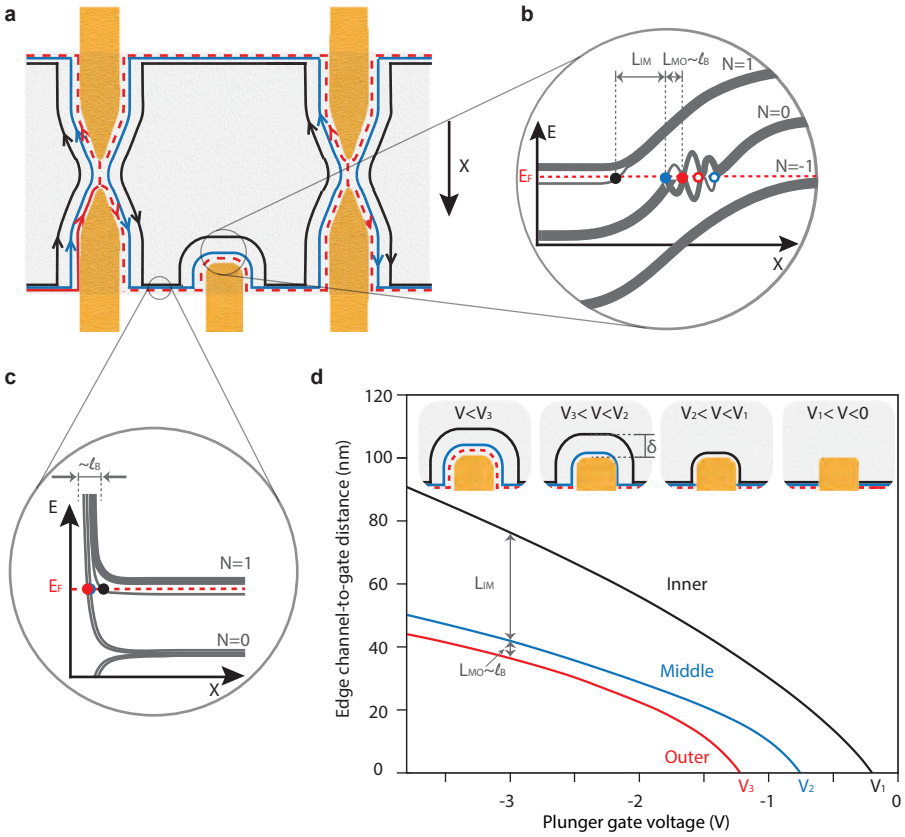

FIG. 5: Interferometric edge channel-to-gate distance determination. a, Schematics of the FPI illustrating interference with the outer edge channel partitioned. Black, blue and red lines represent the inner, middle and outer edge channels, respectively. The FPI edges are gate-defined around the quantum point contact split gates and the plunger gate (color-coded in yellow) and crystal edge-defined for the rest. **b** and **c**, Schematics of the energy dispersion of the Landau levels at $\nu = 3$ along gate-defined (**b**) and crystal-defined (**c**) edges, highlighting noticeable differences in edge positions. The crystal edge dispersion has been assessed in Refs. [23, 25], revealing edge channels confined on the scale of few magnetic lengths from the crystal edge. At the pn junction in **b**, gaps of broken symmetry states open in the zeroth Landau level when the local filling factor $\nu(x)$ reaches every quarter filling, that is, $\nu(x) = -1$, 0, and 1 (Refs. [26, 27]). **d**, Edge channel-to-plunger gate distance for three edge channels, obtained by integrating each plunger gate frequency dispersion in Fig. 4c, as a function of plunger gate voltage. Outer and middle channels are spatially separated by a distance noted L_{MO} that is less than a magnetic length l_B, whereas the inner is at a distance $L_{\mathrm{IM}} \sim 35$ nm from the middle due to the large cyclotron gap between the zeroth and first Landau levels. Details of the experimental distance calculation are provided in the Methods.

on co-propagating channels [31, 32]. If they are strong enough, they decompose electrons into fast (charged) and slow (neutral) modes which split in the two channels. A recent theoretical work on isolated edges predicts that neutral modes produced by an electron entering the FPI could correlate with the tunneling of a second electron, leading to an effective attractive interaction and, consequently, to pairing [12]. While the generalization of such a process to three channels with the correlation of three charges is yet to be demonstrated, it remains the only available suggestion of a pairing mechanism in a QH FPI thus far.

A different explanation of the frequency doubling and tripling based on charging effects [33, 34], which has long obscured Aharonov-Bohm interferometry [20], certainly deserves careful consideration. In our FPI at $\nu = 2$, we observed, for the inner channel, a noteworthy crossover from the Coulomb-dominated (CD) regime to the Aharonov-Bohm (AB) regime , with an increase in the filling factor on the $h/2e$ quantum Hall plateau, as illustrated in Extended Data Figure 2. Simultaneously, the pairing phenomena gets weaker (stronger) when the inner channel is CD-dominant (AB-dominant) (see Extended Data Figure 1 a, b, c, d). Moreover, in our previous study [8], a larger QH FPI with a size of 15, μm^2 demonstrated pairing exclusively at $\nu = 2$, without the presence of additional frequencies (see Fig. S2). In that case, no signatures of the CD regime were observed, most likely

due to a smaller charging energy. Although the question remains open, these concordant observations suggest that the CD regime –charging effects– is not related to the pairing and tripling, in agreement with the conclusions of Ref. [4].

Besides, it is worth mentioning a recent report on pairwise electron tunneling into large quantum dots [35], reminiscent of the FPI configuration. In this context, some theoretical models predict a possible attraction –pairing– of localized electrons resulting from the minimization of the screened Coulomb interaction [36], and even three electrons bunching in very specific configurations [37].

The possibility of bunching three electrons evokes Efimov's physics [38] in which three body bound-states form by contact interaction in vacuum, as well as quarks with color charges that bind to form fermionic hadrons [39]. Such a bunching also resonates with various recent predictions, such as a Fermi liquid of electron trimers transiently induced by optical pumping in superconductors [40], or Cooper trimers in three-component Fermi gases [41, 42]. Our findings, therefore, open up new questions for exploring the three-body problem of interacting electrons with QH edge channels.

Note: During the preparation of this manuscript, we became aware of a work [43] reporting a similar frequency doubling in graphene QH PFI, which is interpreted in terms of capacitive charging of the localized inner channel.

METHODS

Sample fabrication

The hBN-encapsulated graphene heterostructure were assembled from exfoliated flakes using the van der Waals pick-up technique [22] and deposited onto a graphite flake serving as the back-gate electrode. The substrates are highly doped Si wafers with a 285 nm thick SiO_2 layer. The flake thicknesses are 27 nm for the graphite, 45.5 nm for the bottom hBN, and 27.5 nm for the top hBN. Contacts and electrostatic gates were patterned using e-beam lithography, and Cr/Au were deposited for the contacts after etching the heterostructure with a CHF_3/O_2 plasma. Pd was deposited for the electrostatic gates, preceded by a slight O_2 plasma etching to remove resist residues on hBN and ensure a homogeneous electrostatic potential beneath the gate.

Measurements

All measurements were performed in a dilution fridge with a base temperature of 0.01 K at 14T. The measurement setup and filtering is described in [8] and [25]. Systematic current-voltage characteristics were measured in a four terminal configuration as illustrated in Fig. 1a with an acquisition card that oversamples at $\sim 30-50$ kHz for fast averaging. The diagonal voltage drop across the interferometer was measured with a differential FET amplifier. Differential resistance data were obtained by numerically differentiating the current-voltage characteristics. All room-temperature low-noise pre-amplifiers were thermalized in a homemade, temperature-controlled box to get rid of thermal drifts of input voltage offsets.

Checkerboard pattern with harmonics

In a presence of a single harmonics numbered n, the oscillation dependence with bias voltage can be described by the functional form [8]:

$$G_n^{\rm osc} = A_n \left[\beta \cos\left(n \times \left(2\pi \frac{\varphi}{\phi_0} - \frac{2L}{\hbar v} eV\beta \right) \right) + \overline{\beta} \cos\left(n \times \left(2\pi \frac{\varphi}{\phi_0} + \frac{2L}{\hbar v} eV\beta \right) \right) \right] \exp\left(-\frac{(eV)^2}{\sigma_n^2} \right), \quad (1)$$

where β and $\overline{\beta}$ are asymmetry parameters describing how symmetric is the voltage drop on the two side of the interferometer. A_n is the nth harmonic oscillation amplitude. eV is the voltage applied between source and drain. L is the length of the interfering channel between two QPCs, v the edge channel velocity, φ is the Aharonov-Bohm flux picked up by the electrons. The phenomenological Gaussian energy decay describing phase fluctuations of the interfering edge channel due to Coulomb interactions or the electric noise in the non-interfering edge channels [44] fits best our data. Checkerboard pattern in Fig. 2b is very well reproduced by the sum of the three first harmonics $G^{\rm osc} = \sum_n G_n^{\rm osc}$, with $\beta = 0.4$, $\overline{\beta} = 0.6$, $A_1 = 0.25e^2/h$, $A_2 = 0.052e^2/h$, $A_3 = 0.0125e^2/h$, $\sigma_1 = 100$ μeV, $\sigma_2 = 80$ μeV, and $\sigma_3 = 65$ μeV, as shown in Fig. 2c.

Gate-to-edge channel distance from gate-spectroscopy

The gate-spectroscopy is a direct measure of the capacitance coupling between the gate and the interfering edge channels [8]. Assuming a distance δ between the gate and the interfering channel as drawn in the left inset in Fig. 5d, the lever arm of the gate is given by $\alpha(V_{\rm pg}) = L_{\rm pg} \frac{{\rm d}\delta(V_{\rm pg})}{{\rm d}V_{\rm pg}}$, where $L_{\rm pg} = 1.5$ μm is the gate edge length [8]. As a result, one can compute the displacement distance δ by integrating the gate-voltage dependence of the frequency of the considered channel: $\delta(V_{\rm pg}) = \frac{\phi_0}{BL_{\rm pg}} \int_{V_{\rm pg}^{\rm c}}^{V_{\rm pg}} f_{\rm pg}(V){\rm d}V$, using $\Delta A = \phi_0/B = \alpha \Delta V_{\rm pg} = \alpha/f_{\rm pg}$. Fig. 5d displays the resulting distances for the three channels at $\nu = 3$ computed from Fig. 4c.

Evolution of electron pairing with filling factor

The relative contributions of the outer edge channel and pairing to the interference signal vary with the filling factor when partitioning the outer edge channel on the $h/2e$ quantum Hall plateau. On the left side of the plateau, at $V_{\rm bg} = 1.2$ V ($\nu = 1.7$), the interference signal is dominated by the outer edge channel contribution, as observed in Extended Data Fig. 1a and c. In the middle of the plateau, at $V_{\rm bg} = 1.58$ V ($\nu = 2$), the contributions from the outer edge channel and pairing are comparable, as shown in Extended Data Fig. 1b and d. On the right side of the plateau, at $V_{\rm bg} = 1.8$ V ($\nu = 2.26$), the pairing contribution becomes dominant, as illustrated in Fig. 3a and b. It's important to note that the precise weighting of the outer channel and pairing contributions is bias voltage-dependent, as evident in Extended Data Fig. 1d-g.

Coulomb dominated to Aharonov-Bohm dominated transition on the inner edge

We present in this section and in Extended Data Fig. 2 the continuous evolution of inner edge channel interferences from Coulomb dominated to Aharonov-Bohm type when increasing filling factor on the $h/2e$ plateau [20]. The magnetic field periodicity of the inner edge channel interference continuously evolves as the filling factor is increased as shown in Extended Data Fig. 2b. On the left of the plateau, the oscillations are completely Coulomb dominated i.e. the period is equal to the Aharonov-Bohm period but with a negative slope of constant phase line on the pajama plot [33] as shown in Extended Data Fig. 2c. On the middle of the plateau, the oscillations are almost magnetic field independent as shown in Extended Data Fig. 2d. On the right side of the plateau, the oscillations correspond to a pure Aharonov-Bohm modulation as shown in main text Fig. 1b. This evolution is consistent with a reduced bulk-inner edge interaction as the filling factor is increased. Note that on the right part of the plateau, the Fermi level is pinned in the Liftshitz tail of the N=1 Landau level such that the bulk compressible island is separated from the edge channels by a distance similar to that assessed in Fig. 5d. On the contrary, on the left part of the plateau, the Fermi level in pinned at the top of the zeroth LL, which forms a compressible island of localized states that are potentially closer to the edge channels.

ACKNOWLEDGMENTS

We thank A. Assouline, D. Basko, P. Degiovanni, M. Heiblum, B. Rosenow, K. Snizhko and E. Sukhorukov for valuable discussions. We thank F. Blondelle for technical support on the experimental apparatus. Samples were prepared at the Nanofab facility of the Néel Institute. This work has received funding from the European Union's Horizon 2020 research and innovation program under the ERC grant *SUPERGRAPH* No. 866365. B.S., H.S. and W.Y. acknowledge support from the QuantERA II Program that has received funding from the European Union's Horizon 2020 research and innovation program under Grant Agreement No 101017733. K.W. and T.T. acknowledge support from the JSPS KAKENHI (Grant Numbers 20H00354, 21H05233 and 23H02052) and World Premier International Research Center Initiative (WPI), MEXT, Japan.

[1] M. Tinkham, Introduction to Superconductivity (Dover Publications, 2004).
[2] A. Hamo, A. Benyamini, I. Shapir, I. Khivrich, J. Waissman, K. Kaasbjerg, Y. Oreg, F. von Oppen, and S. Ilani, Electron attraction mediated by Coulomb repulsion, Nature **535**, 395 (2016).
[3] C. Hong, G. Yoo, J. Park, M.-K. Cho, Y. Chung, H.-S. Sim, D. Kim, H. Choi, V. Umansky, and D. Mahalu, Attractive Coulomb interactions in a triple quantum dot, Physical Review B **97**, 241115 (2018).
[4] H. Choi, I. Sivan, A. Rosenblatt, M. Heiblum, V. Umansky, and D. Mahalu, Robust electron pairing in the integer quantum Hall effect regime, Nature Communications **6**, 7435 (2015).
[5] I. Sivan, R. Bhattacharyya, H. Choi, M. Heiblum, D. Feldman, D. Mahalu, and V. Umansky, Interaction-induced interference in the integer quantum Hall effect, Physical Review B **97**, 125405 (2018).
[6] J. Nakamura, S. Fallahi, H. Sahasrabudhe, R. Rahman, S. Liang, G. C. Gardner, and M. J. Manfra, Aharonov–Bohm interference of fractional quantum Hall edge modes, Nature Physics **15**, 563 (2019).
[7] S. Biswas, H. K. Kundu, V. Umansky, and M. Heiblum, Electron Pairing of Interfering Interface-Based Edge Modes, Physical Review Letters **131**, https://doi.org/10.1103/PhysRevLett.131.096302 (2023).
[8] C. Déprez, L. Veyrat, H. Vignaud, G. Nayak, K. Watanabe, T. Taniguchi, F. Gay, H. Sellier, and B. Sacépé, A tunable Fabry–Pérot quantum Hall interferometer in graphene, Nature Nanotechnology **16**, 555 (2021).
[9] Y. Ronen, T. Werkmeister, D. Haie Najafabadi, A. T. Pierce, L. E. Anderson, Y. J. Shin, S. Y. Lee, Y. H. Lee, B. Johnson, K. Watanabe, et al., Aharonov–Bohm effect in graphene-based Fabry–Pérot quantum Hall interferometers, Nature Nanotechnology **16**, 563 (2021).
[10] L. Zhao, E. G. Arnault, T. F. Larson, Z. Iftikhar, A. Seredinski, T. Fleming, K. Watanabe, T. Taniguchi, F. Amet, and G. Finkelstein, Graphene-based quantum Hall interferometer with self-aligned side gates, Nano Letters **22**, 9645 (2022).

[11] H. Fu, K. Huang, K. Watanabe, T. Taniguchi, and J. Zhu, Charge Oscillations in Bilayer Graphene Quantum Confinement Devices, Nano Letters **23**, 9726 (2023).

[12] G. A. Frigeri and B. Rosenow, Electron pairing in the quantum Hall regime due to neutralon exchange, Physical Review Research **2**, 043396 (2020).

[13] D. B. Chklovskii, B. I. Shklovskii, and L. I. Glazman, Electrostatics of edge channels, Physical Review B **46**, 4026 (1992).

[14] Z. F. Ezawa and G. Tsitsishvili, Quantum Hall ferromagnets, Reports on Progress in Physics **72**, 086502 (2009).

[15] B. I. Halperin and J. K. Jain, Fractional Quantum Hall Effects: New Developments (World Scientific, 2020).

[16] C. Nayak, S. H. Simon, A. Stern, M. Freedman, and S. D. Sarma, Non-Abelian anyons and topological quantum computation, Reviews of Modern Physics **80**, 1083 (2008).

[17] B. Van Wees, L. P. Kouwenhoven, C. Harmans, J. Williamson, C. Timmering, M. Broekaart, C. Foxon, and J. Harris, Observation of zero-dimensional states in a one-dimensional electron interferometer, Physical Review Letters **62**, 2523 (1989).

[18] D. Ferraro and E. Sukhorukov, Interaction effects in a multi-channel Fabry-Pérot interferometer in the Aharonov-Bohm regime, SciPost Physics **3**, 014 (2017).

[19] G. A. Frigeri, D. D. Scherer, and B. Rosenow, Subperiods and apparent pairing in integer quantum Hall interferometers, Europhysics Letters **126**, 67007 (2019).

[20] Y. Zhang, D. T. McClure, E. M. Levenson-Falk, C. M. Marcus, L. N. Pfeiffer, and K. W. West, Distinct signatures for Coulomb blockade and Aharonov-Bohm interference in electronic Fabry-Perot interferometers, Physical Review B **79**, 241304 (2009).

[21] K. Zimmermann, A. Jordan, F. Gay, K. Watanabe, T. Taniguchi, Z. Han, V. Bouchiat, H. Sellier, and B. Sacépé, Tunable transmission of quantum Hall edge channels with full degeneracy lifting in split-gated graphene devices, Nature Communications **8**, 14983 (2017).

[22] L. Wang, I. Meric, P. Y. Huang, Q. Gao, Y. Gao, H. Tran, T. Taniguchi, K. Watanabe, L. M. Campos, D. A. Muller, J. Guo, P. Kim, J. Hone, K. L. Shepard, and C. R. Dean, One-dimensional electrical contact to a two-dimensional material, Science **342**, 614 (2013).

[23] A. Coissard, A. G. Grushin, C. Repellin, L. Veyrat, K. Watanabe, T. Taniguchi, F. Gay, H. Courtois, H. Sellier, and B. Sacépé, Absence of edge reconstruction for quantum Hall edge channels in graphene devices, Science Advances **9**, eadf7220 (2023).

[24] W. Yang, D. Perconte, C. Déprez, K. Watanabe, T. Taniguchi, S. Dumont, E. Wagner, F. Gay, I. Safi, H. Sellier, and B. Sacépé, Supplementary Videos for Evidence for correlated electron pairs and triplets in quantum Hall interferometers, Zenodo https://doi.org/10.5281/zenodo.10420556 (2023).

[25] H. Vignaud, D. Perconte, W. Yang, B. Kousar, E. Wagner, F. Gay, K. Watanabe, T. Taniguchi, H. Courtois, Z. Han, H. Sellier, and B. Sacépé, Evidence for chiral supercurrent in quantum Hall Josephson junctions, Nature **624**, 545 (2023).

[26] X. Liu, G. Farahi, C.-L. Chiu, Z. Papic, K. Watanabe, T. Taniguchi, M. P. Zaletel, and A. Yazdani, Visualizing broken symmetry and topological defects in a quantum Hall ferromagnet, Science **375**, 321 (2022).

[27] A. Coissard, D. Wander, H. Vignaud, A. G. Grushin, C. Repellin, K. Watanabe, T. Taniguchi, F. Gay, C. B. Winkelmann, H. Courtois, H. Sellier, and B. Sacépé, Imaging tunable quantum Hall broken-symmetry orders in graphene, Nature **605**, 51 (2022).

[28] I. Safi, A dynamic scattering approach for a gated interacting wire, Eur. Phys. J. B. **12**, 451 (1999).

[29] K.-V. Pham, M. Gabay, and P. Lederer, Fractional excitations in the Luttinger liquid, Phys. Rev. B **61**, 16397 (2000).

[30] I. P. Levkivskyi and E. V. Sukhorukov, Dephasing in the electronic Mach-Zehnder interferometer at filling factor $\nu = 2$, Phys. Rev. B **78**, 045322 (2008).

[31] E. Berg, Y. Oreg, E.-A. Kim, and F. von Oppen, Fractional Charges on an Integer Quantum Hall Edge, Phys. Rev. Lett. **102**, 236402 (2009).

[32] H. Inoue, A. Grivnin, N. Ofek, I. Neder, M. Heiblum, V. Umansky, and D. Mahalu, Charge fractionalization in the integer quantum Hall effect, Physical Review Letters **112**, 166801 (2014).

[33] B. I. Halperin, A. Stern, I. Neder, and B. Rosenow, Theory of the Fabry-Pérot quantum Hall interferometer, Physical Review B **83**, 155440 (2011).

[34] I. Sivan, H. Choi, J. Park, A. Rosenblatt, Y. Gefen, D. Mahalu, and V. Umansky, Observation of interaction-induced modulations of a quantum Hall liquid's area, Nature communications **7**, 12184 (2016).

[35] A. Demir, N. Staley, S. Aronson, S. Tomarken, K. West, K. Baldwin, L. Pfeiffer, and R. Ashoori, Correlated Double-Electron Additions at the Edge of a Two-Dimensional Electronic System, Physical Review Letters **126**, 256802 (2021).

[36] M. E. Raikh, L. I. Glazman, and L. E. Zhukov, Two-Electron State in a Disordered 2D Island: Pairing Caused by the Coulomb Repulsion, Physical Review Letters **77**, 1354 (1996).

[37] R. Putnam Jr and M. E. Raikh, Three-electron bunches in occupation of a Coulomb cluster with N= 5 sites, Physical Review B **104**, 195425 (2021).

[38] P. Naidon and S. Endo, Efimov physics: a review, Reports on Progress in Physics **80**, 056001 (2017).

[39] W. Marciano and H. Pagels, Quantum chromodynamics, Physics Reports **36**, 137 (1978).

[40] A. Sanayei, P. Naidon, and L. Mathey, Electron trimer states in conventional superconductors, Phys. Rev. Res. **2**, 013341 (2020).

[41] P. Niemann and H.-W. Hammer, Pauli-blocking effects and Cooper triples in three-component Fermi gases, Phys. Rev. A **86**, 013628 (2012).

[42] S. Akagami, H. Tajima, and K. Iida, Condensation of Cooper triples, Phys. Rev. A **104**, L041302 (2021).

[43] T. Werkmeister, J. R. Ehrets, Y. Ronen, M. E. Wesson, D. Najafabadi, Z. Wei, K. Watanabe, T. Taniguchi, D. E. Feldman, B. I. Halperin, A. Yacoky, and P. Kim, Strongly coupled edge states in a graphene quantum Hall interferometer, arXiv preprint arXiv:2312.03150 https://doi.org/10.48550/arXiv.2312.03150 (2023).

[44] P. Roulleau, F. Portier, D. Glattli, P. Roche, A. Cavanna, G. Faini, U. Gennser, and D. Mailly, Finite bias visibility of the electronic Mach-Zehnder interferometer, Physical Review B **76**, 161309 (2007).

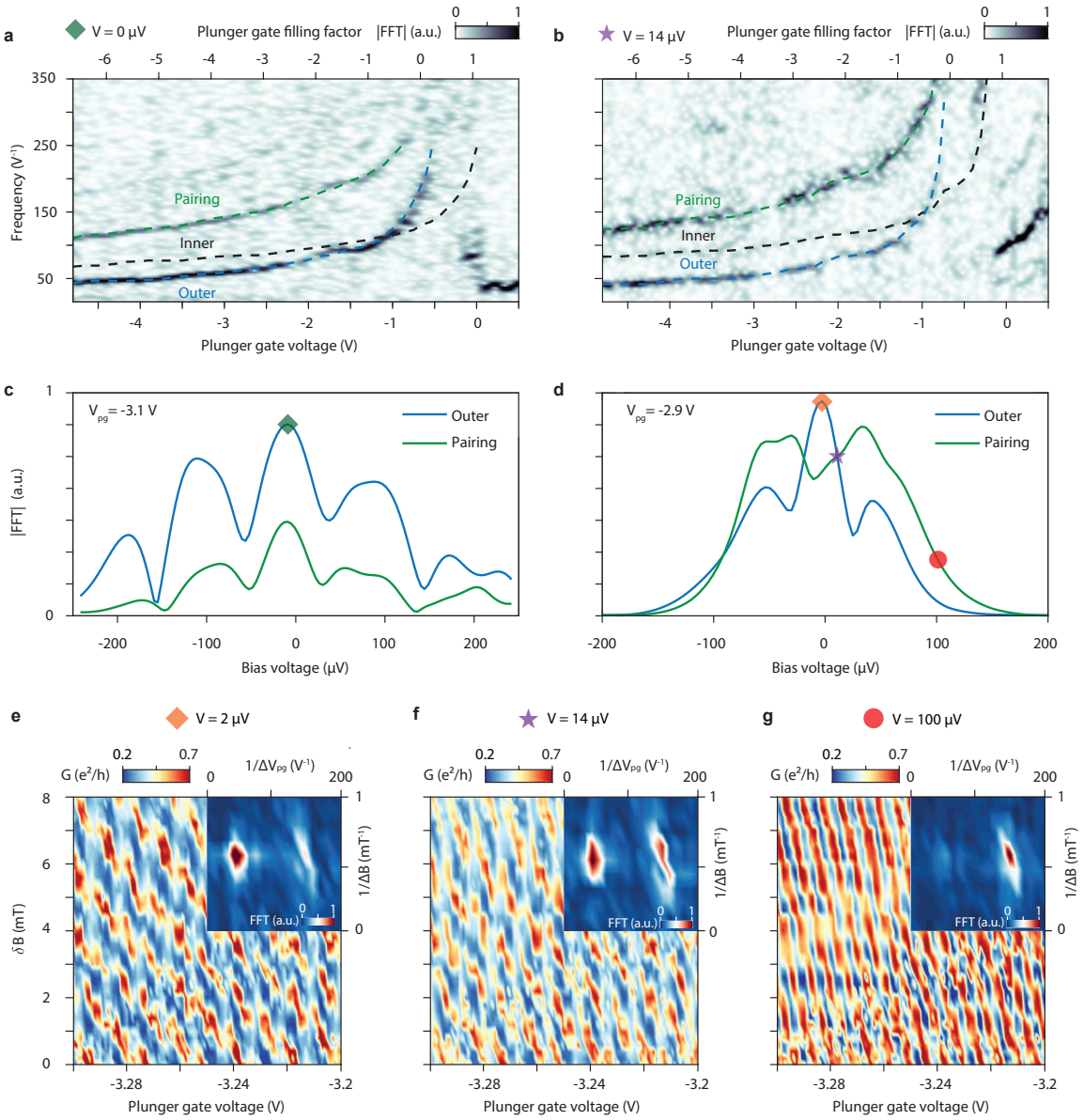

Extended Data Fig. 1: Electron pairing evolution with filling factor and bias voltage for outer edge channel partial transmission. a-b. FT amplitude obtained from oscillations when partially transmitting the outer channel at $V_{\mathrm{bg}} = 1.2$ V and $V_{\mathrm{bg}} = 1.58$ V, versus plunger gate voltage and oscillation frequency. Black dash lines are taken from interference of inner channel. Blue dash lines guide the frequency of outer channel interference, and green dash lines is the sum of the two other frequencies. **c-d.** Lobe structure of paired channel (green colored) and outer channel (blue colored) at $V_{\mathrm{bg}} = 1.2$ V and $V_{\mathrm{bg}} = 1.58$ V. Pairing frequency is dominated over the whole bias ranges at $V_{\mathrm{bg}} = 1.2$ V but is comparable with outer signal at $V_{\mathrm{bg}} = 1.58$ V. **e-g.** Pajama maps of outer channel at $V_{\mathrm{bg}} = 1.58$ V measured at $V_{\mathrm{bias}} = 2\ \mu\mathrm{V}, 14\ \mu\mathrm{V}, 100\ \mu\mathrm{V}$.

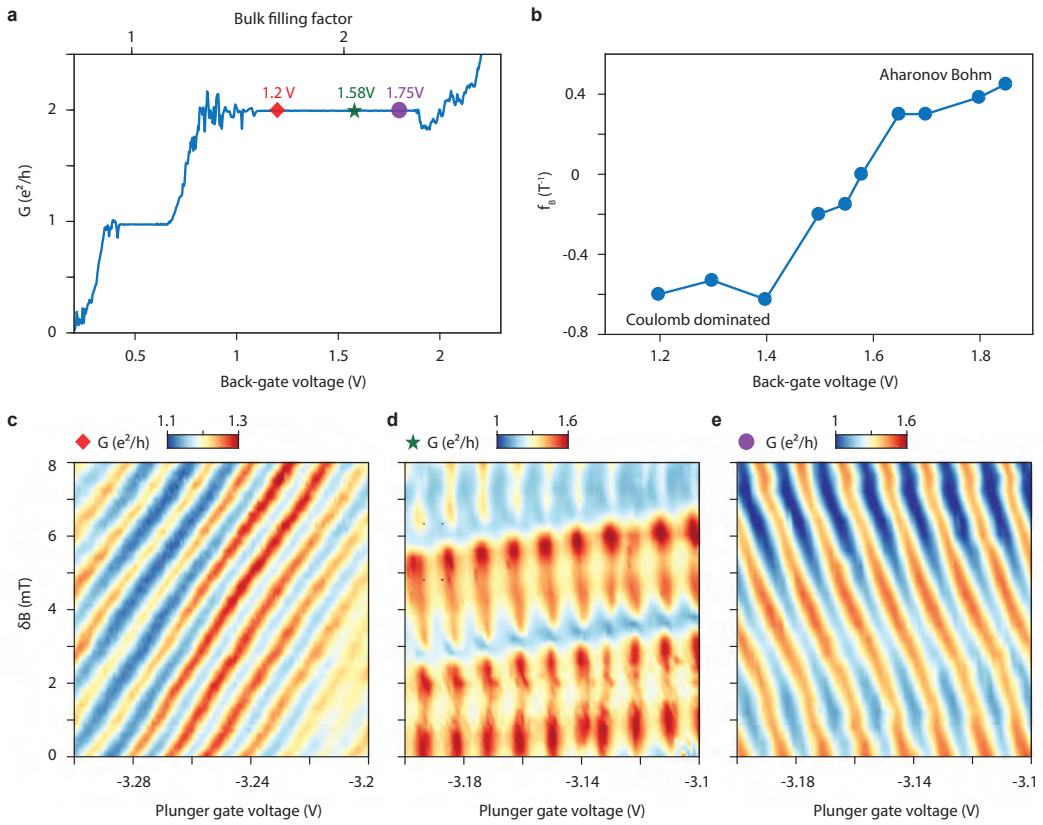

Extended Data Fig. 2: Coulomb dominated to Aharonov-Bohm dominated transition on the inner edge. a. Diagonal conductance across the interferometer as a function of back-gate voltage. The dots indicate the back-gate voltages used in the different panels. **b.** Magnetic field oscillation frequency when pinching the inner edge channel as a function of back-gate voltage, the sign is chosen positive (negative) when the constant phase line have a positive (negative) slope in the pajama map. **c-e.** Pajama plot when pinching the inner edge channel at back-gate voltage of 1.2 V - 1.58 V - 1.75 V, indicated with color marks on the plateau in (a).

Supplementary Information

I. QUANTUM HALL CHARACTERIZATION

Here we highlight the back-gate voltages corresponding to the bulk filling factors at which the interferometry experiments were performed. Figure S1 shows the diagonal conductance of device WY50 of the main text, measured in the configuration shown in Fig. 1a. Integer quantum Hall states, including broken symmetry states, are well developed as featured by quantized diagonal conductance when sweeping the back-gate voltage at 14 T. We summarize below the back-gate voltages $V_{\rm bg}$ (indicated by colored dots in Fig. S1) and corresponding bulk filling factors ν for all figures of the work.

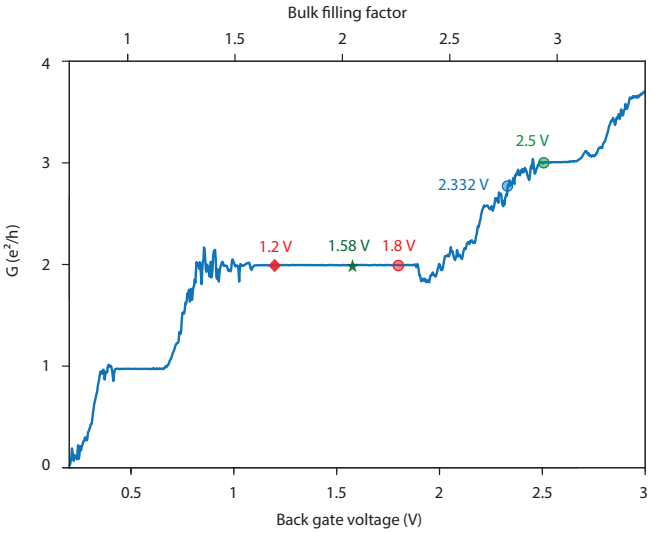

Fig. S1: Quantum Hall plateaus. Diagonal conductance of device WY50 of the main text as a function of back-gate voltage at 14 T. Top axis is the bulk filling factor. The dots on the quantum Hall plateau indicate the back-gate voltage where each figure was measured: $V_{\rm bg} = 1.2$ V ($\nu = 1.7$, red diamond), $V_{\rm bg} = 1.58$ V ($\nu = 2$, green star),$V_{\rm bg} = 1.8$ V ($\nu = 2.26$, red dot). For higher filling factor, we present data obtained at $V_{\rm bg} = 2.33$ V ($\nu = 2.8$, blue dot) and $V_{\rm bg} = 2.5$ V ($\nu = 2.93$, green dot).

- $V_{\rm bg} = 1.2$ V ($\nu = 1.7$) : Ext. Data. Figs. 1a,c and 2a,c (red diamond in Fig. S1).
- $V_{\rm bg} = 1.58$ V ($\nu = 2$): Ext. Data. Figs. 1b,d and 2b,d-g (green star in Fig. S1).
- $V_{\rm bg} = 1.8$ V ($\nu = 2.26$) : Figs. 1-3 and Fig. S3 and Supplementary Videos 1-4 [24] (red dot in Fig. S1).
- $V_{\rm bg} = 2.33$ V ($\nu = 2.8$) : Fig. S5 and Supplementary Videos 8-10 [24] (blue dot in Fig. S1).
- $V_{\rm bg} = 2.5$ V ($\nu = 2.9$) : Figs. 4 and 5 and Supplementary Videos 5 and 6 [24] (green dot in Fig. S1).

II. EVOLUTION OF PAIRING STRENGTH WITH INTERFEROMETER SIZE

Here, we present additional data obtained from sample BNGr74 comprising two interferometers in series, which was extensively studied in [8]. This device configuration allows to study, in the same sample, three interferometers of different sizes: 3.1 μm^2, 10.7 μm^2 and 14.7 μm^2. The measurements were performed with standard lock-in at zero-bias voltage. Figs. S2a-c exhibit the gate spectroscopy of the outer edge channel as a function of plunger gate voltage in small, medium and large interferometers, respectively. The pairing signal is more pronounced in the medium interferometer and is present alone in the large interferometer where charging effects are expected to be lessened, indicating an anti-correlation between charging energy and the emergence of the pairing frequency.

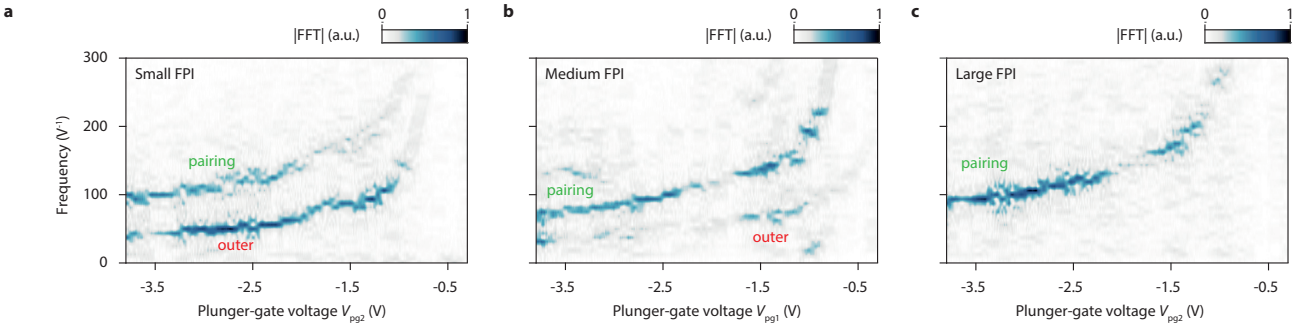

Fig. S2: Evolution of pairing strength with interferometer size. Fourier transform amplitude of conductance oscillations versus plunger gate voltage and plunger gate frequency when partitioning the outer edge channel at $\nu = 2$. **a**, Small FPI of 3.1 μm^2 is measured at $\nu = 2.3$. **b**, Medium FPI of 10.7 μm^2 is measured at $\nu = 2.3$. **c**, Large FPI of 14.7 μm^2 is measured at $\nu = 2.5$.

III. EDGE CHANNEL-TO-PLUNGER GATE DISTANCE AT $\nu = 2$

We estimate the displacement of the edge channels with respect to the plunger gate edge, $\delta(V_{\rm pg})$, at $V_{\rm bg} = 1.8$ V, that is, $\nu = 2.26$. The calculation details are described in the Methods. Figure S3d shows the edge displacement for both inner and outer edge channels versus plunger gate voltage, computed with the frequency dispersions shown in Fig. 3a. For $V_{\rm pg} > V_1$ corresponding to a filling factor higher than 1 below the plunger gate, both inner and outer channels propagate along the crystal edge underneath the plunger gate as schematically depicted in Fig. S3c. Upon decreasing the gate voltage below V_1, the inner channel rapidly shifts towards the interior of the interferometer cavity as illustrated in Fig. S3b. Subsequently, the outer channel quickly moves towards the inner side of the plunger gate when pinching plunger gate at the critical voltage V_2, corresponding to filling factor 0 below the plunger gate, as illustrated in Fig. S3a.

IV. LOBE STRUCTURE AT $\nu = 3$

We show in Fig. S4 the Fourier transform amplitude –lobe structure– as a function of dc bias voltage extracted from Fig. 4. Fourier transform amplitudes are related to the pairing, tripling and inner channels (extracted from Fig. 4c) in Fig. S4a, and to inner and middle channels (extracted from Fig. 4d) in Fig. S4b. Contrary to the harmonics observed for inner edge channel interferences in Fig. 2f, here, all Fourier transform amplitudes exhibit comparable periodicities in bias voltage. The extracted Thouless energies, of the order of 100 μV, are comparable to that of the inner edge channel shown in Fig. 2. This indicates a similar order of magnitude for the velocity of each edge channel.

V. TRIPLING AT ANOTHER BULK FILLING FACTOR

Fig. S5 shows the interference behavior observed at $V_{\rm bg} = 2.33$ V ($\nu_{\rm B} = 2.8$) involving three edge channels, similar to the data presented in Fig. 4. Figs. S5a-c show the dependence of Fourier transform amplitude on plunger gate voltage at zero bias, extracted from conductance oscillations when partitioning the inner, middle and outer edge

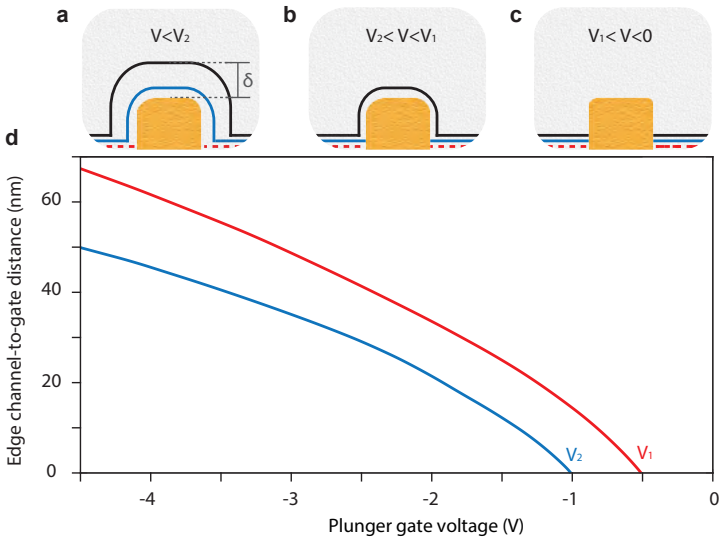

Fig. S3: Edge channel-to-plunger gate distance at $\nu = 2$. a-c, Schematics of the edge channel configurations in three different plunger gate regimes, where δ represents the distance between the edge channel and the plunger gate. **d**, Edge channel-to-plunger gate distance for the inner and outer channels at $V_{\mathrm{bg}} = 1.8$ V, extracted from the plunger gate frequency dispersions in Fig. 3a.

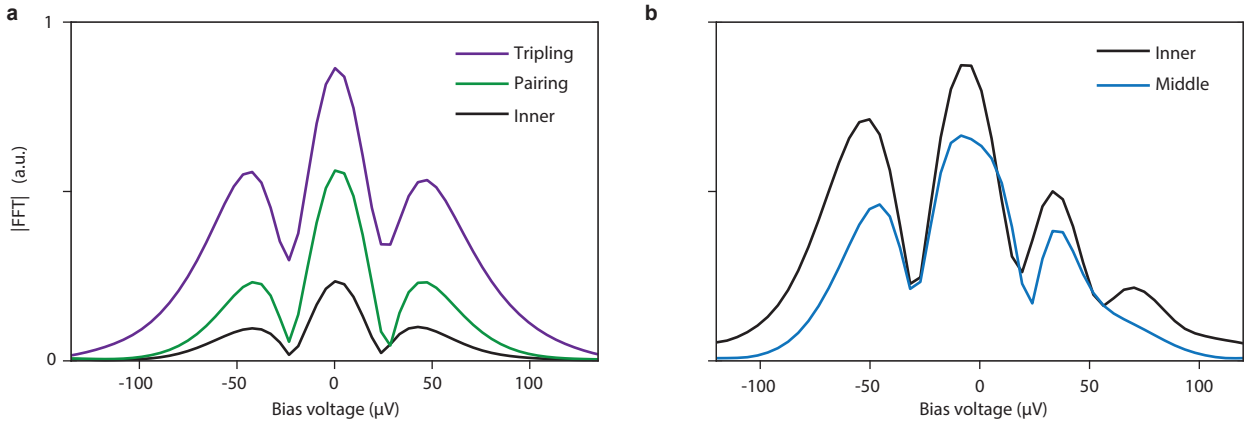

Fig. S4: Lobe structure of edge channels at $\nu = 3$. **a**, Lobe structures of the Fourier transform amplitude for the inner channel and pairing (between middle and outer channels) and tripling when partitioning the outer edge channel at $V_{\mathrm{bg}} = 2.5$ V, corresponding to the data in Fig. 4c. **b**, Lobe structures of the inner and middle edge channels when partitioning the middle channel, corresponding to the data in Fig. 4d.

channels, respectively. Similar to Fig. 4, electron pairing and tripling clearly emerge when interfering with the middle and outer edge channels. Figs. S5d-f present the pajama maps, revealing Coulomb-dominated oscillations in the inner channel interference (Fig. S5d) and complex patterns involving multiple frequencies for both middle (Fig. S5e) and outer (Fig. S5f) edge channel interference.

Interestingly, the inner channel interference in Fig. S5d exhibits CD regime for all bias voltages as shown in the SI Video 8 [24]. On the other hand, the exact regime for the middle channel interference can be evaluated in the SI Video 9 [24], where at high bias, an AB regime dominates and can be attributed to the middle channel through its plunger gate periodicity. Around zero bias the pattern shown in Fig. S5e is a mixture of the middle AB, a weaker contribution of the inner CD and pairing. For outer channel interference in Fig. S5f, the energy dependence of the pajama does not help distinguish individual channel contributions.

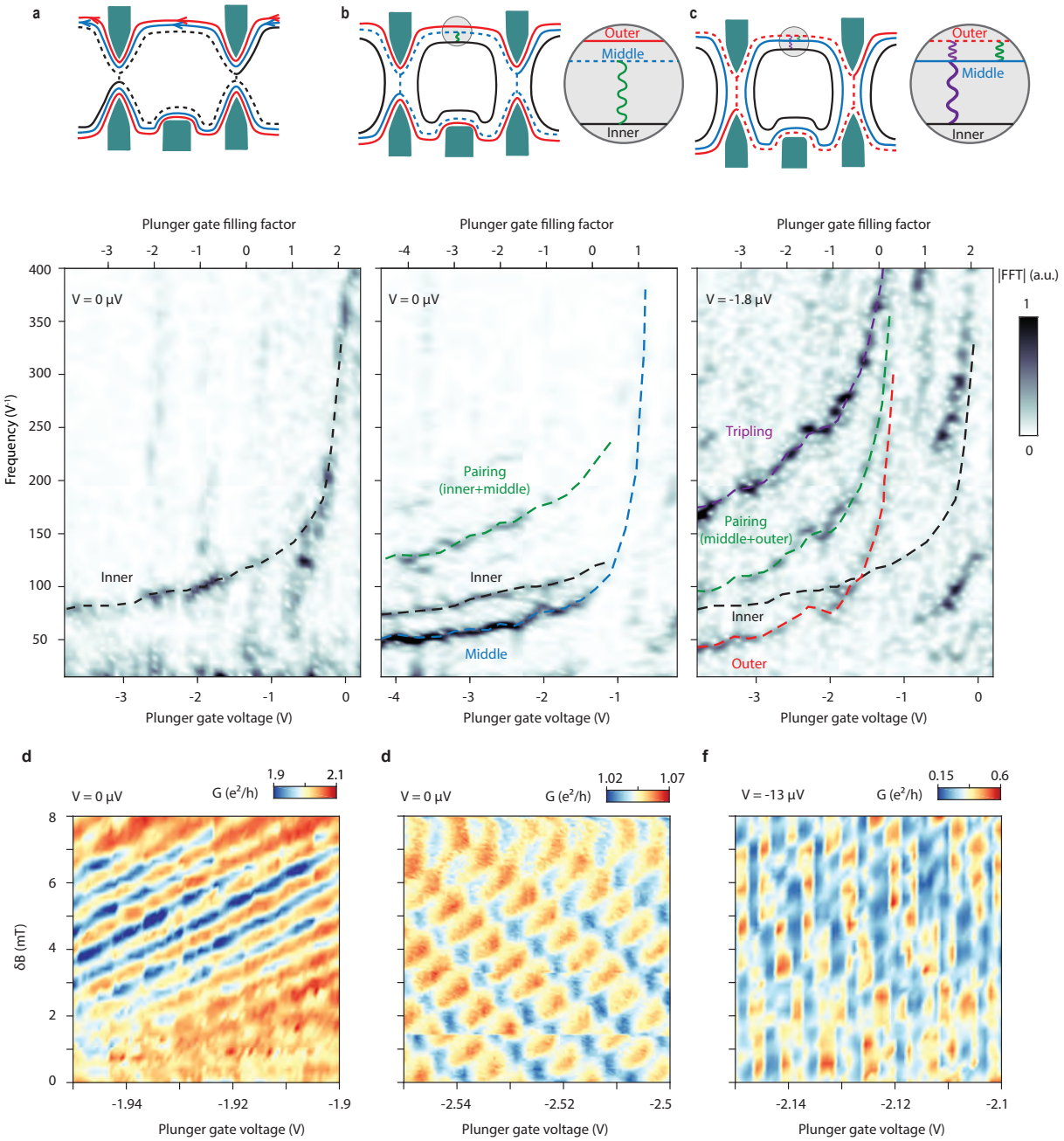

Fig. S5: Interference pattern at $V_{\mathrm{bg}} = 2.33$ V ($\nu = 2.8$). **a**, Fourier transform of conductance oscillation versus plunger gate voltage when partitioning the inner edge channel. The oscillation exhibits a single frequency. **b**, When partitioning the middle edge channel, three frequency dispersions can be associated with the inner (dashed black line), middle (dashed blue line) and the sum frequency of inner and middle (dashed green line). **c.** When partitioning the outer edge channel, the low frequency dispersion is related to the outer edge (red black line), and the moderate signal is the sum frequency of outer and middle (pairing, dashed green line). The strongest frequency dispersion is associated with the sum frequency of all three channels (purple green line). **d-f**, Pajama maps showing conductance oscillations for partitioning of inner, middle and outer edges, respectively. Here the data are shown at zero bias extracted from the IV curves.

VI. SUPPLEMENTARY VIDEOS [24]

A. SI Video 1 (complement to Fig. 2d): Bias voltage evolution of the inner edge channel conductance oscillation

Conductance oscillation as a function of plunger gate voltage when partitioning the inner channel (as depicted in Fig. 2d) extracted for each voltage from the IV curves [24].

B. SI Video 2 (complement to Fig. 2e): Bias voltage evolution of the inner edge channel gate-spectroscopy

Bias voltage dependence of the Fourier transform of Fig. 2e as a function of plunger gate voltage when partitioning the inner edge channel. The Fourier transform is computed with the data of SI Video 1 [24].

C. SI Video 3 (complement to Fig. 3a): Bias voltage evolution of the outer edge channel gate-spectroscopy

Bias voltage dependence of the Fourier transform of Fig. 3a as a function of plunger gate voltage when partitioning the outer edge channel [24].

D. SI Video 4 (complement to Fig. 3c): Bias voltage evolution of the outer edge channel pajama map

Pajama map is extracted for each voltage from the IV curves, showcasing the partitioning of the outer channel (as demonstrated in Fig. 3c) [24]. The beating pattern aligns with the lobe structure of Fig. 3b (the lobe structure extracted from the pajama is almost identical). At high (positive or negative) voltage, a single frequency (tripling) dominates with a small modulation on top. Around ± 65 μV, the two frequencies have similar amplitudes, and the pajama looks like a checkerboard. Around -30 μV, the pairing signal dominates, and the pajama is similar to the one at high (positive or negative) voltage. Around 0 μV, the pajama pattern is akin to the one in Fig. 3c, with one dominating oscillation (pairing) but periodically interrupted by a second smaller oscillation stemming from the outer edge channel.

E. SI Video 5 (complement to Fig. 4c): Bias voltage evolution of the outer edge channel (tripling) gate-spectroscopy

Conductance oscillations with plunger gate voltage, obtained by partitioning the outer edge channel at filling factor 3 (as in Fig. 4c) [24], are extracted for each voltage from the IV curves. At high (positive or negative) voltage, a single frequency (tripling) is visible. Around ± 65 μV, a second lower frequency appears, which corresponds to the pairing of the middle and outer channels. Around ± 30 μV, two additional frequencies appear, corresponding to the middle and outer edge channel oscillations. Around ± 20 μV, all four amplitudes are fainter, corresponding to the first minimum of the lobe structure. Around ± 0 μV, one recovers Fig. 4c. Similar to Supplementary Video 3, all three signals appear and disappear with comparable frequency (in bias voltage), in agreement with the lobe structure of Fig. S4a. Note that the different frequency dispersions are independent of bias voltage.

F. SI Video 6 (complement to Fig. 4d): Bias voltage evolution of the middle edge channel (tripling) gate-spectroscopy

Conductance oscillations with plunger gate voltage, obtained by partitioning the middle edge channel at filling factor 3 (as in Fig. 4d) [24], are extracted for each voltage from the IV curves. At high (positive or negative) voltage, two signals of comparable amplitude are visible, corresponding to middle and inner edge channel oscillations. As the voltage is increased, both two amplitudes increase, while a new pairing signal appears around ± 55 μV. Around ± 0 μV, one recovers the map of Fig. 4d. Similar to supplementary videos 3 and 5, middle and inner signals appear and disappear with comparable frequency (in bias voltage), in agreement with the lobe structure of Fig. S4b. Note that the different frequency dispersions are independent of bias voltage.

G. SI video 7 : Bias voltage evolution of the outer edge channel pajama at $V_{\rm bg} = 2.6$ V

Conductance oscillations with plunger gate voltage and magnetic field, obtained by partitioning the inner edge channel at filling factor 3.1 (as in Fig. S5d) [24], are extracted for each voltage from the IV curve. At high (positive or negative) voltage, the interference pattern exhibits a negative slope in the B-$V_{\rm pg}$ plane, characteristic of Coulomb-dominated interference due to a contribution from the inner edge channel. Between ± 80 μV, the outer channel, pairing (of middle and outer), and tripling can contribute to the interference. The pajama pattern thus changes with bias voltage depending on which channel is dominating.

H. SI video 8 (complement to Fig. S5d): Bias voltage evolution of the inner edge channel pajama at $V_{\rm bg} = 2.33$ V

Pajama map, obtained by partitioning the inner edge channel at filling factor 3 (as in Fig. S5d), are extracted for each voltage from the IV curve [24]. The interference pattern exhibits a negative slope in the B-$V_{\rm pg}$ plane, characteristic of Coulomb-dominated interference. The interference pattern is nearly independent of bias voltage. The slight modifications in the pattern with bias voltage are primarily attributed to changes in visibility.

I. SI video 9 (complement to Fig. S5e): Bias voltage evolution of the middle edge channel pajama at $V_{\rm bg} = 2.33$ V

Pajama map, obtained by partitioning the middle edge channel at filling factor 3 (as in Fig. S5e), are extracted for each voltage from the IV curve [24]. As illustrated in Fig. S5e, interference from the inner channel, the middle channel, and their pairing can occur in this scenario. The pajama pattern thus varies with bias voltage, depending on which channel is dominating at a given voltage. At high (positive or negative) voltage, the middle edge channel dominates, giving rise to an Aharonov-Bohm dominated pajama. As the voltage is increased, the inner channel appears (Coulomb dominated) and introduces an extra modulation around ± 110 μV. Around ± 77 μV, the pairing channel appears, dominating the overall low-visibility interference pattern. Around ± 50 μV, the middle channel dominates the oscillations with a small modulation due to pairing. Around 0 μV, all channels are present with low visibility.

J. SI video 10 (complement to Fig. S5f): Bias voltage evolution of the outer edge channel pajama at $V_{\rm bg} = 2.33$ V

Conductance oscillations with plunger gate voltage and magnetic field, obtained by partitioning the middle edge channel at filling factor 3 (as in Fig. S5f) [24], are extracted for each voltage from the IV curve. As illustrated in Fig. S5f, interference from the outer channel, the pairing (involving the middle and outer channels), and the tripling can occur in this scenario. The pajama pattern thus varies with bias voltage, depending on which channel is dominating at a given voltage.